Supporting Information

A Metal-on-Metal Growth Approach to Metal-Metal Oxide Core-Shell Nanostructures with Plasmonic Properties

Cameron C. Crane,[†] Ryan H. Manso,[†] Jun Li,[‡] Mourad Benamara,[§] Jing Tao,[‡] Yimei Zhu,[‡] Feng Wang,[†] Jingyi Chen[†,*]

[†]Department of Chemistry and Biochemistry, University of Arkansas, Fayetteville, AR 72701

[‡]Condensed Matter Physics and Materials Science Department, Brookhaven National Laboratory, Upton, NY 11973

[§]Institute of Nanoscience and Engineering, University of Arkansas, Fayetteville, AR 72701

[*]Corresponding author: chenj@uark.edu (+1 479-575-6203)

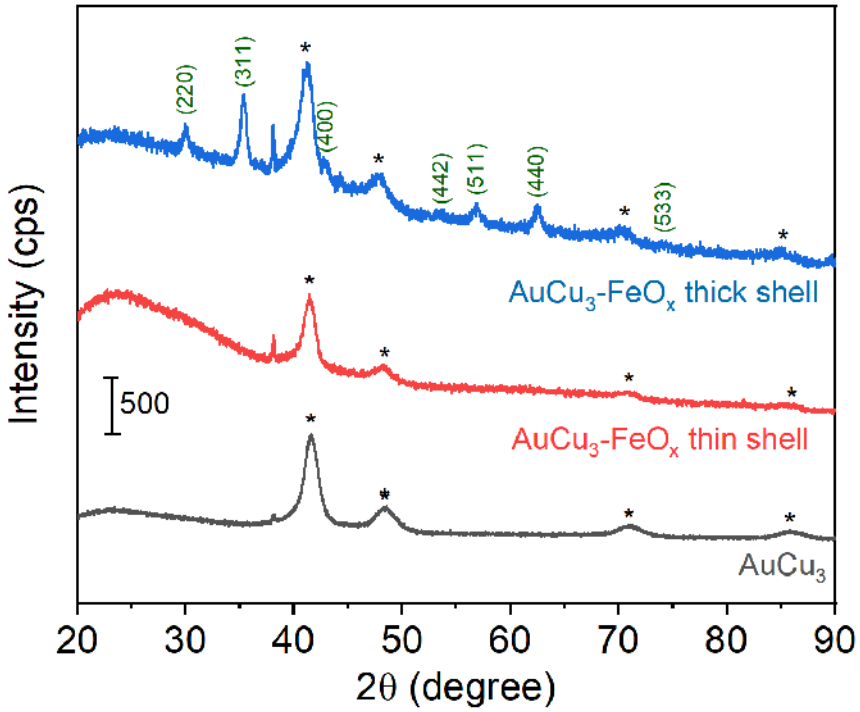

Figure S1. XRD spectra of $AuCu_3$ nanostructures before and after the FeO_x deposition process: $AuCu_3$ nanorods (dark grey), $AuCu_3$-FeO_x core-shell structures with a thin shell (red), and $AuCu_3$-FeO_x core-shell structures with a thick shell (blue). The peaks labelled with "*" are indexed to the (111), (200), (220), and (311) planes of the face-centered-cubic (fcc) $AuCu_3$ alloy. The peaks that are assigned with the Miller indices in green correspond to the XRD pattern of Fe_3O_4 (JCPDS 88-0315).

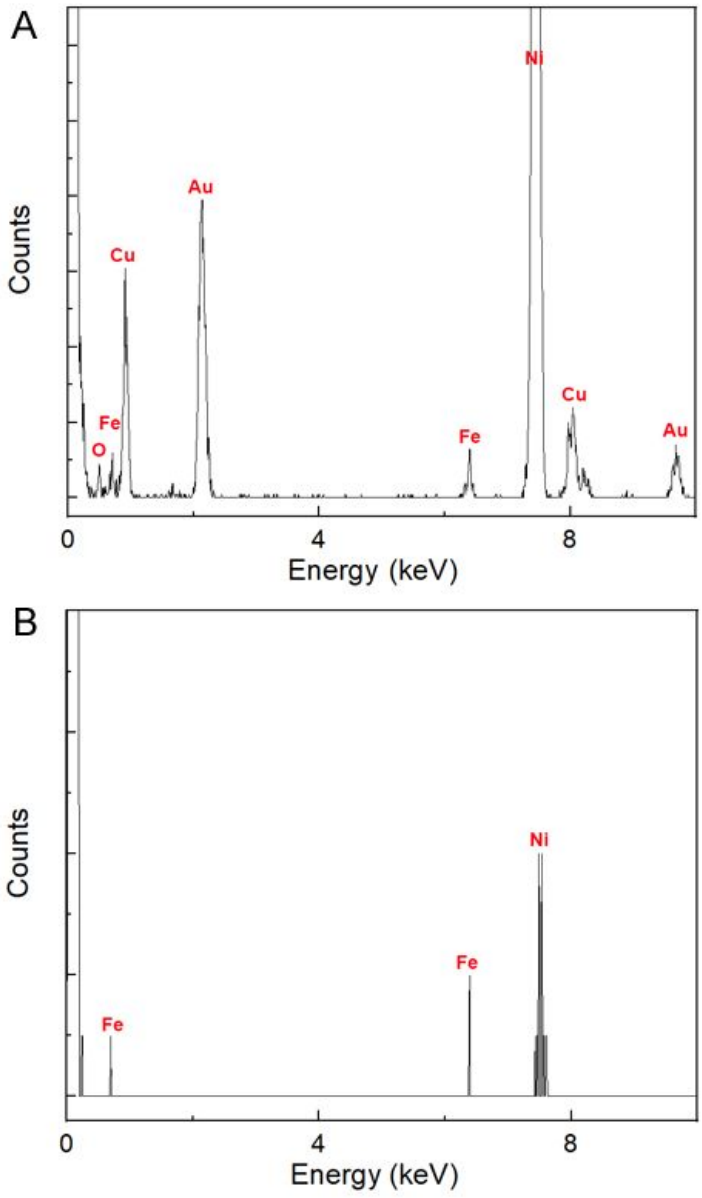

Figure S2. EDX spectral analysis of the $AuCu_3$-FeO_x core-shell nanostructures with a thin shell in Figure 2C: (A) EDX spectrum taken from the entire mapping area; and (B) EDX spectrum obtained from one individual green pixel where Fe is located. These EDX spectra indicate that the EDX signals (Au, Cu, Fe and O) are clearly above the baseline noise. Note that the Ni signals come from the Ni TEM grid where the nanoparticles were deposited.

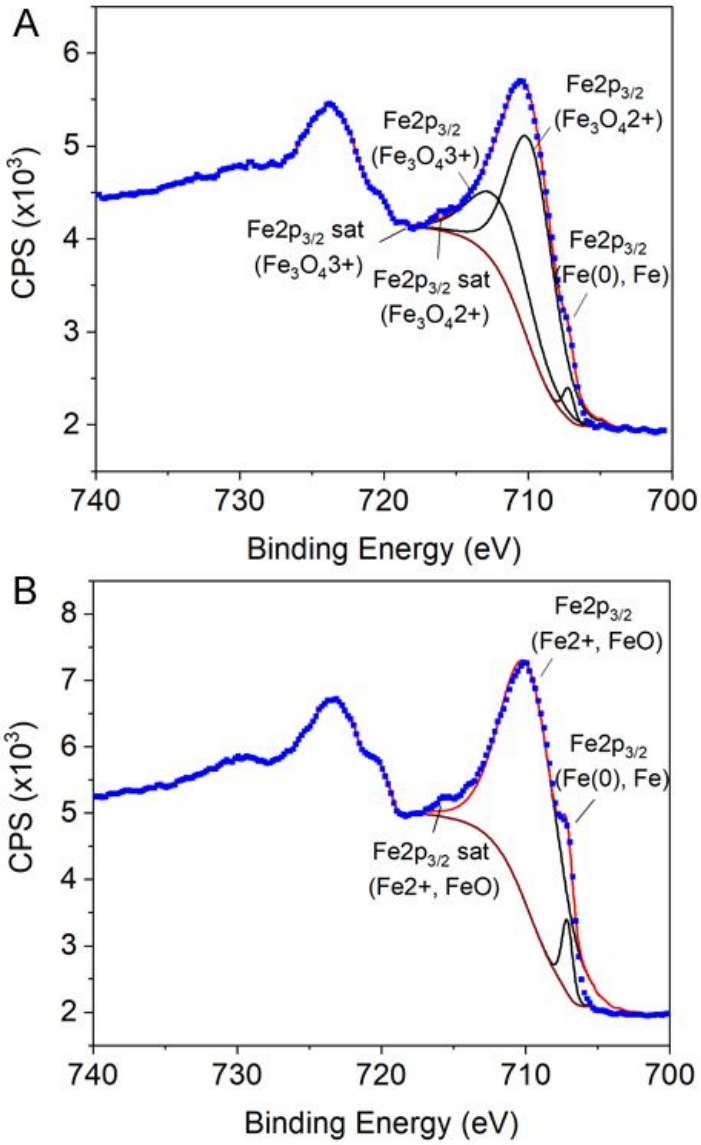

Figure S3. XPS Fe2p spectra of the $AuCu_3$-FeO_x core-shell structures: (A) with a thick shell; and (B) with a thin shell. The experimental data were plotted as dot blue curves. The $Fe2p_{3/2}$ data was fitted using CasaXPS software based on the literature-reported values.[1] The fittings of individual components were plotted in blue and their sum was plotted in red. The baselines were corrected by Shirley method as indicted in brown.

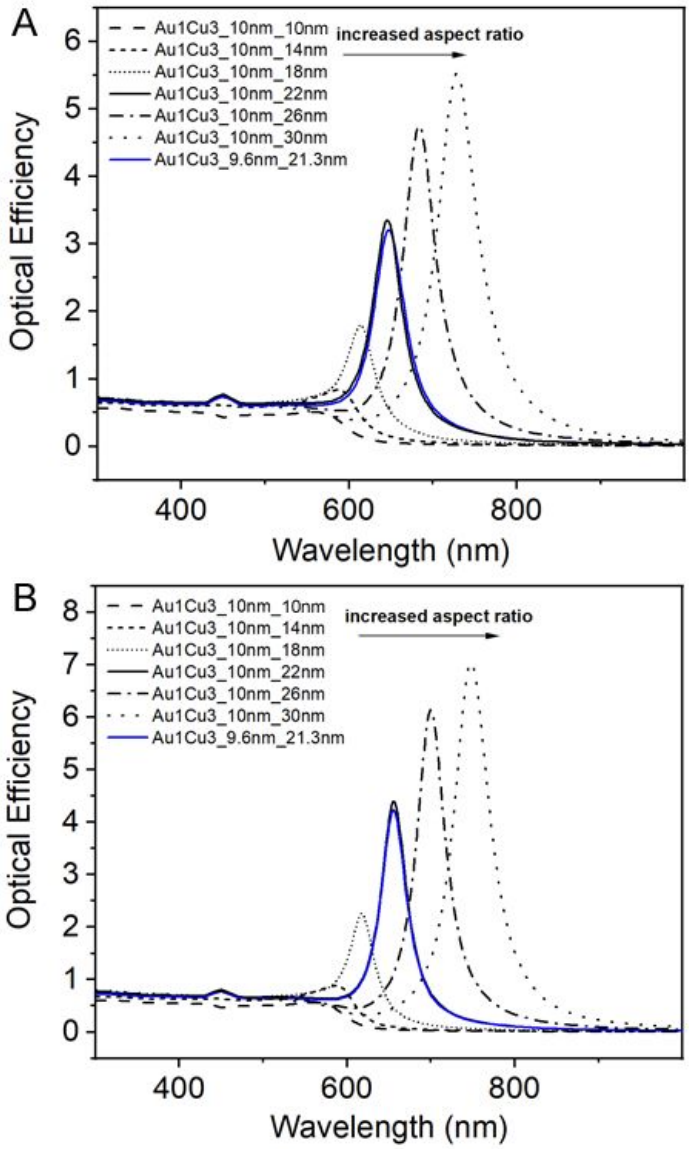

Figure S4. DDA simulations of the $AuCu_3$ nanorods with different aspect ratios at a fixed diameter of 10 nm using two types of targets in the DDSCAT program: (A) ellipsoidal targets; and (B) cylindrical targets (cylinder with hemispherical endcaps). For the aspect ratios studied, cylindrical targets and ellipsoidal targets gave almost identical peak characteristics.

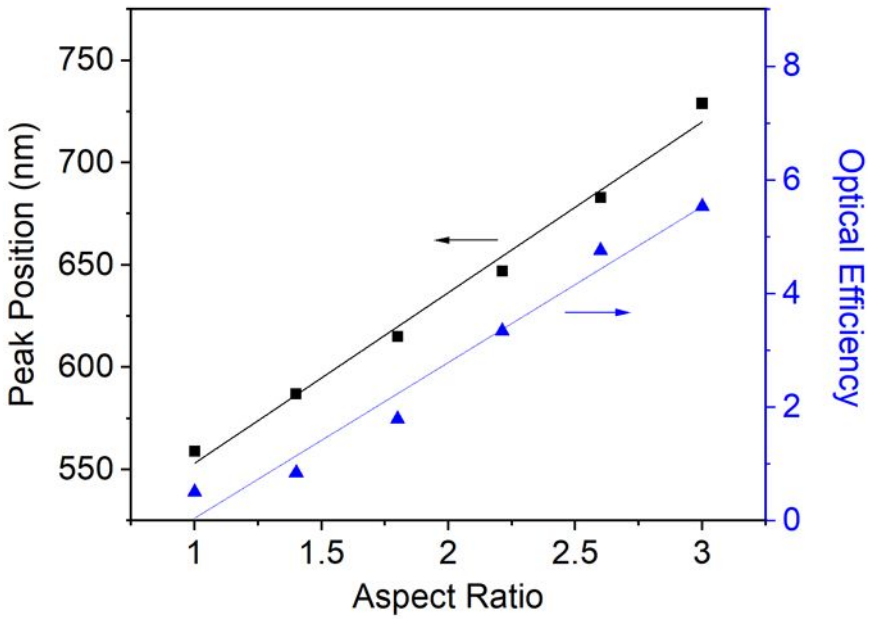

Figure S5. The plot indicating the peak position (square) and optical efficiency (triangle) of the LSPR longitudinal modes of the $AuCu_3$ nanorods shown in Figure 4B as a function of their aspect ratios. The linear fits of the data are plotted as the black curve for the peak position-aspect ratio relationship ($y = 469.6\,\text{nm} + 83.5x$, $R^2 = 0.99$) and the blue curve for the optical efficient-aspect ratio relationship ($y = -2.70 + 2.74x$, $R^2 = 0.97$).

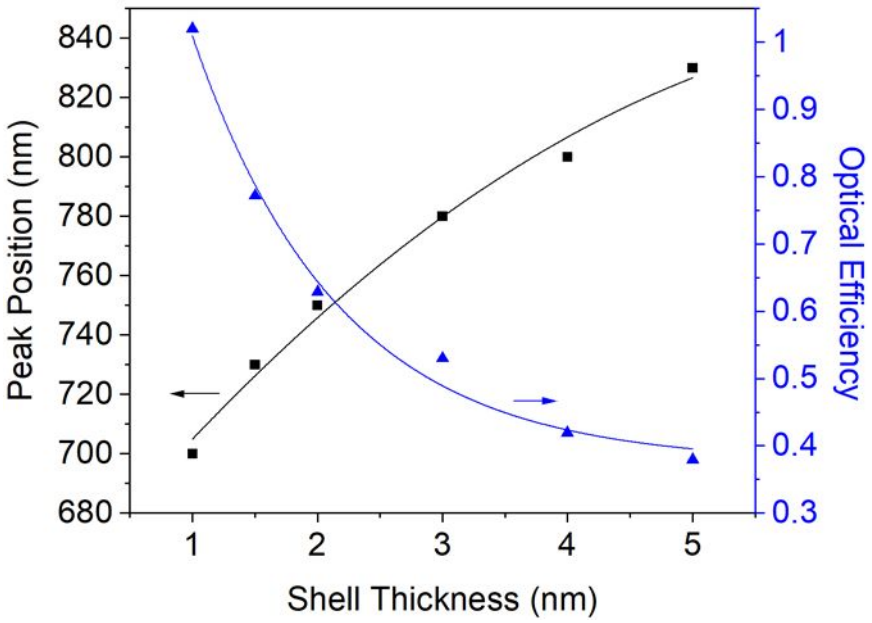

Figure S6. The plot indicating the peak position (square) and optical efficiency (triangle) of the LSPR longitudinal modes of the $AuCu_3$-Fe_3O_4 core-shell nanorods shown in Figure 4C as a function of their Fe_3O_4 shell thickness. The polynomial fit of the data is plotted as the black curve for the peak position-shell thickness relationship ($y = 656.9\ \text{nm} + 51.5x - 3.5x^2$, $R^2 = 0.99$). The exponential fit of the data is plotted as the blue curve for the optical efficient-shell thickness relationship ($y = 0.374 + 1.49e^{-0.856x}$, $R^2 = 0.99$).

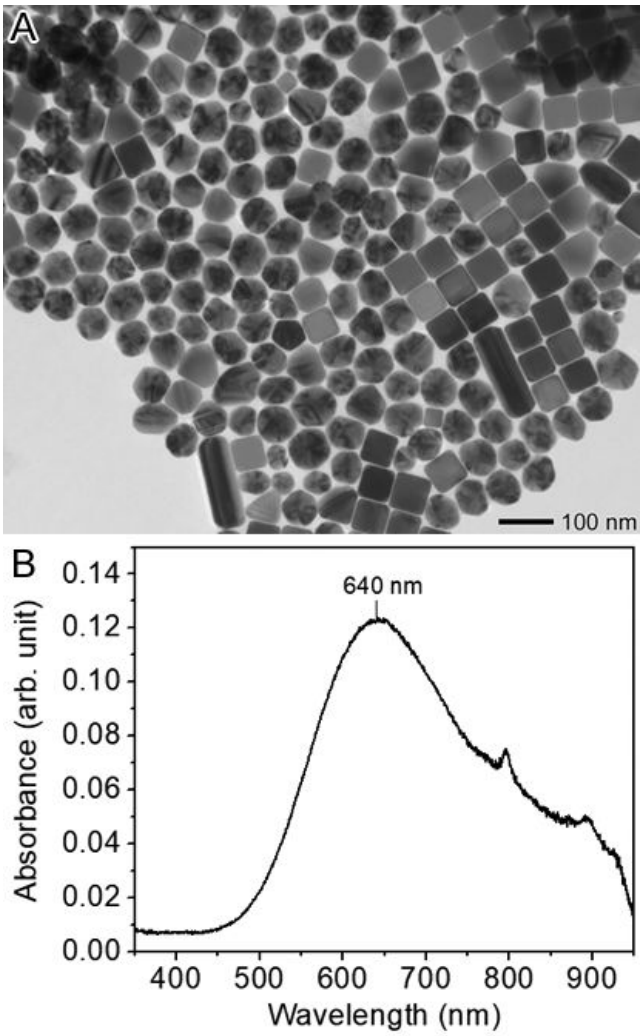

Figure S7. (A) TEM image of Cu nanoparticles; and (B) UV-vis spectrum of the sample is (A) suspended in toluene.

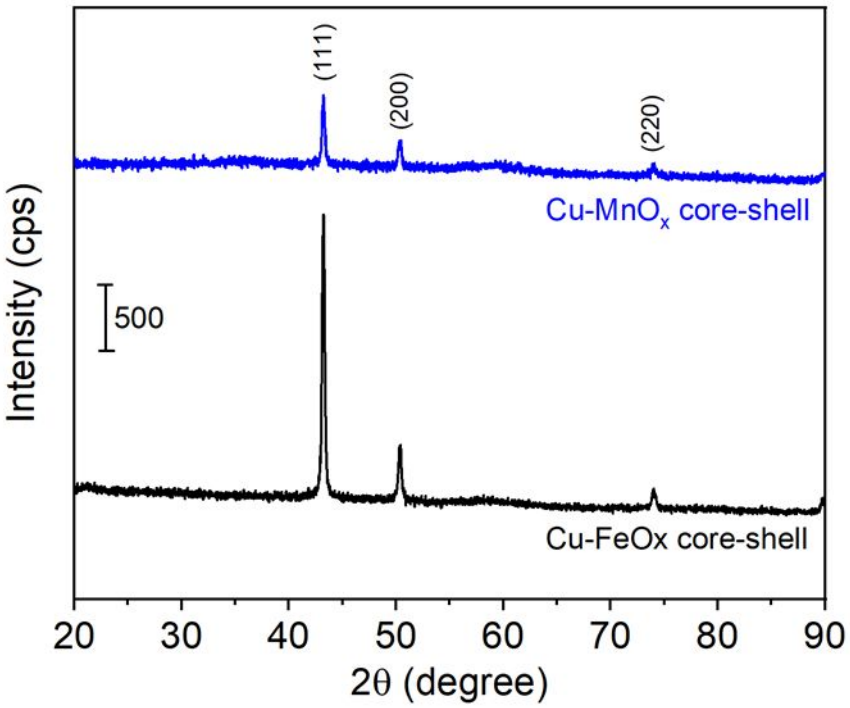

Figure S8. XRD spectra of Cu-FeO_x (black curve) and Cu-MnO_x (blue) core-shell nanostructures. The peaks that are assigned with the Miller indices correspond to the XRD pattern of the fcc Cu (JCPDS 04-0836). The amorphous shells were confirmed as indicated by the lacks of observable patterns other than the pattern of the Cu core fcc crystal structure.

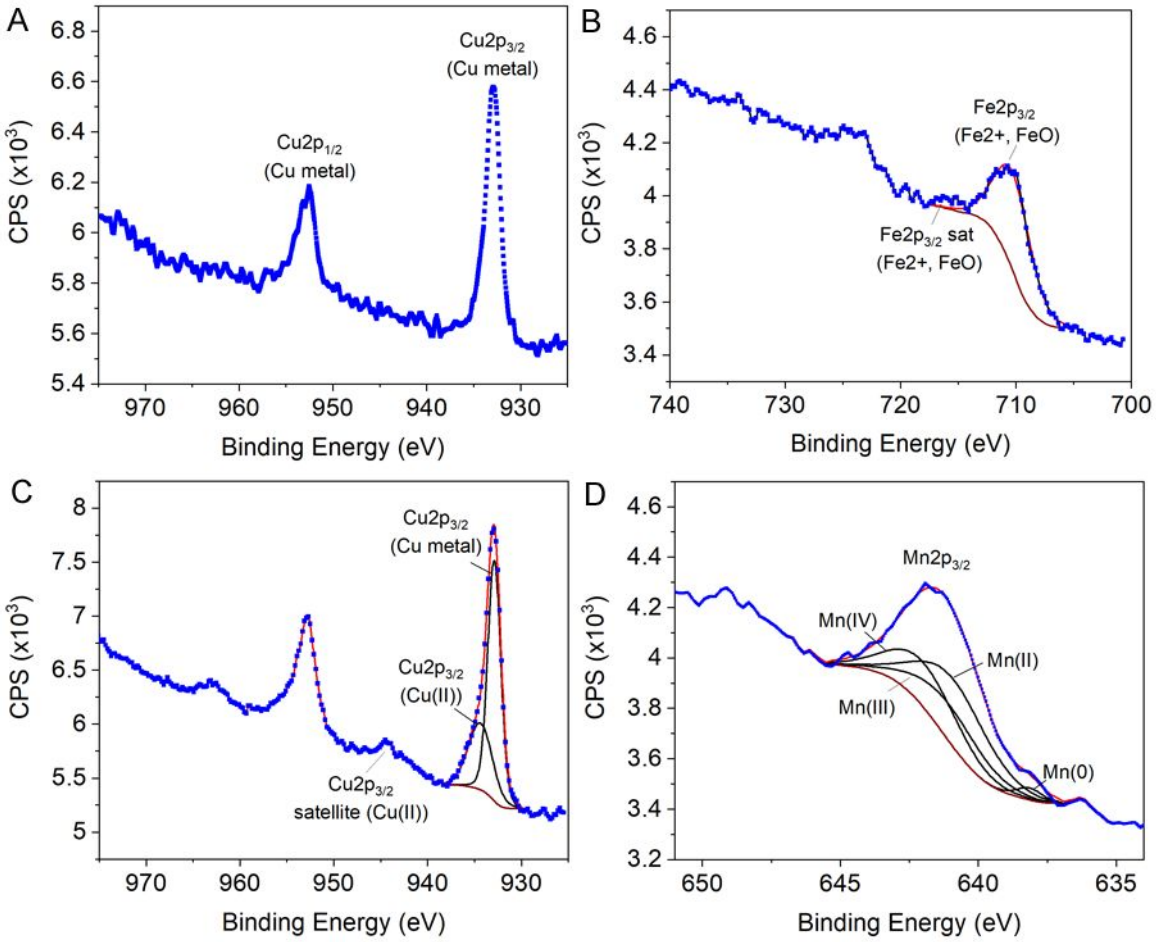

Figure S9. XPS spectra of the core-shell structures of Cu-FeO_x (A: Cu2p; B: Fe2p) and Cu-MnOx (C: Cu2p; D: Mn2p3/2). The experimental data were plotted as dot blue curves. The data was fitted using CasaXPS software based on the literature-reported values.[1-2] The fittings of individual components were plotted in blue and their sum was plotted in red. The baselines were corrected by Shirley method as indicted in brown.

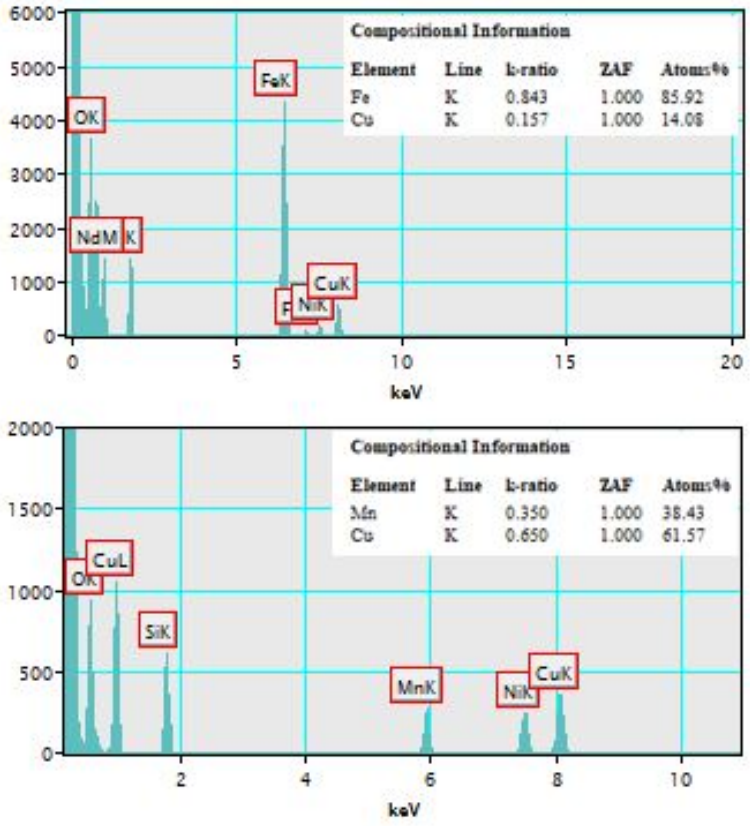

Figure S10. EDX spectra of the hollow mixed oxides: (A) $CuFeO_x$; and (B) $CuMnO_x$. By analyzing the EDX spectra, there are Fe 85.92% and Cu 14.08% in the $CuFeO_x$ hollow structures whereas the $CuMnO_x$ hollow structures contain 38.48% Mn and 61.57% Cu.

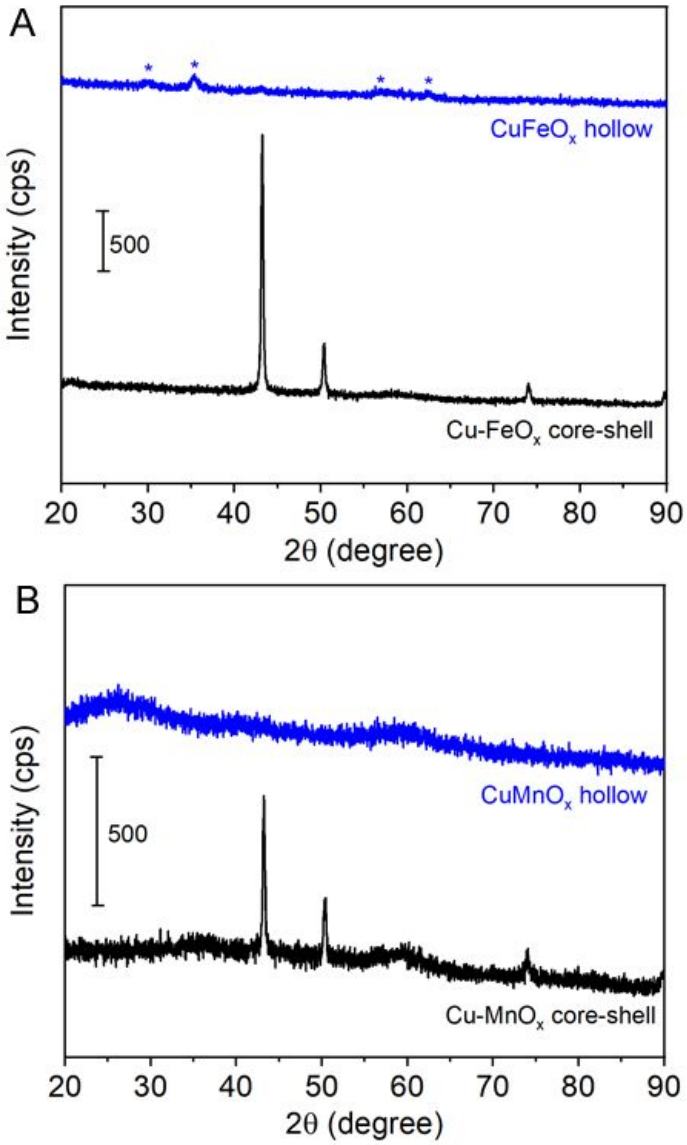

Figure S11. XRD spectra of the $CuFeO_x$ (A) and $CuMnO_x$ (B) hollow nanostructures that are colored in blue with the XRD spectra colored in back corresponding to their core-shell structures as comparison. The Cu fcc pattern disappears in the spectra of the hollow structures, indicating the complete dissolution of the Cu cores by etching the core-shell structures with NH_4OH solution. Note that the peaks labelled by * in the spectrum of $CuFeO_x$ hollow structures can be indexed to the XRD pattern of Fe_3O_4 (JCPDS 88-0315), but the peak intensities are much weaker than those in the thick shell sample (Figure S1) due to poor crystallinity of the thin shell sample.

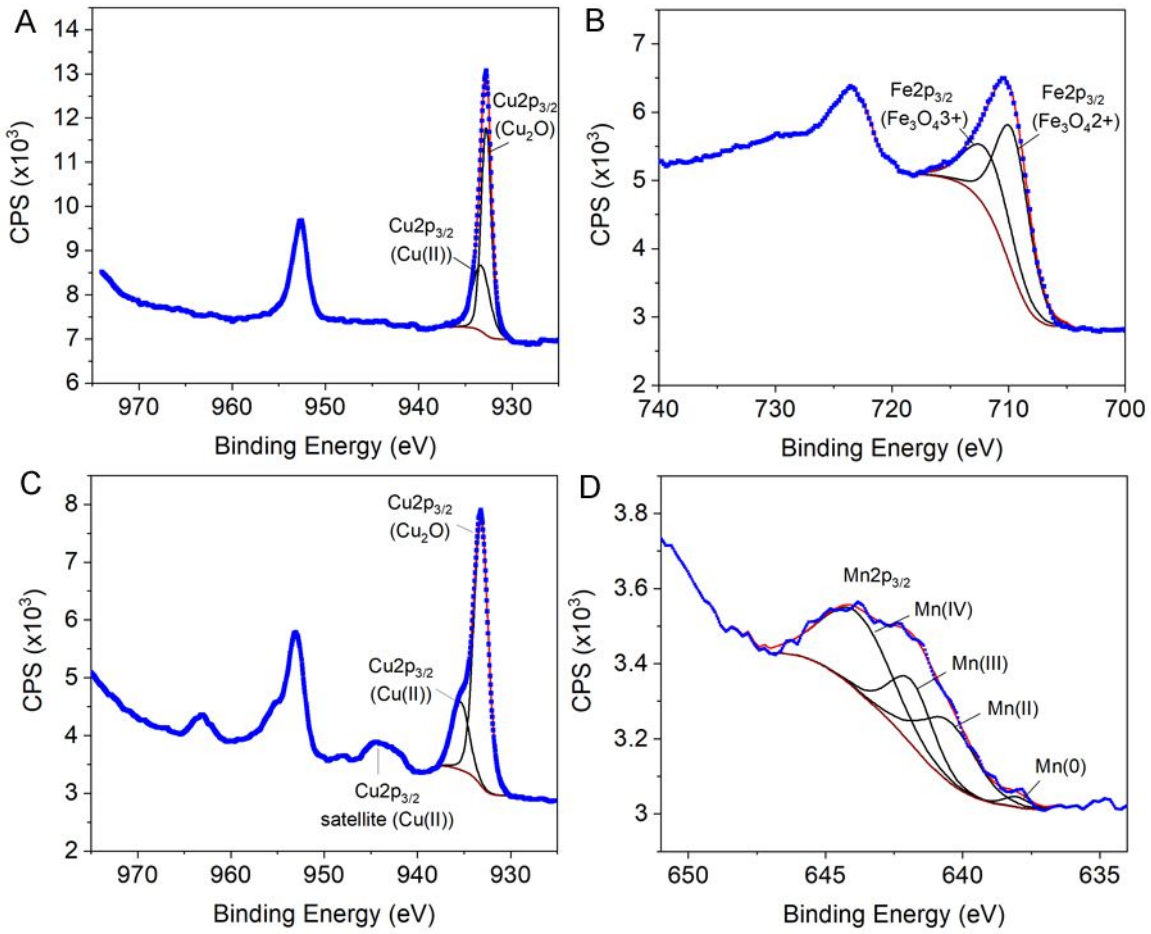

Figure S12. XPS spectra of the hollow structures of $CuFeO_x$ (A: Cu2p; B: Fe2p) and CuMnOx (C: Cu2p; D: Mn2p3/2). The experimental data were plotted as dot blue curves. The data was fitted using CasaXPS software based on the literature-reported values.[1-2] The fittings of individual components were plotted in blue and their sum was plotted in red. The baselines were corrected by Shirley method as indicted in brown.

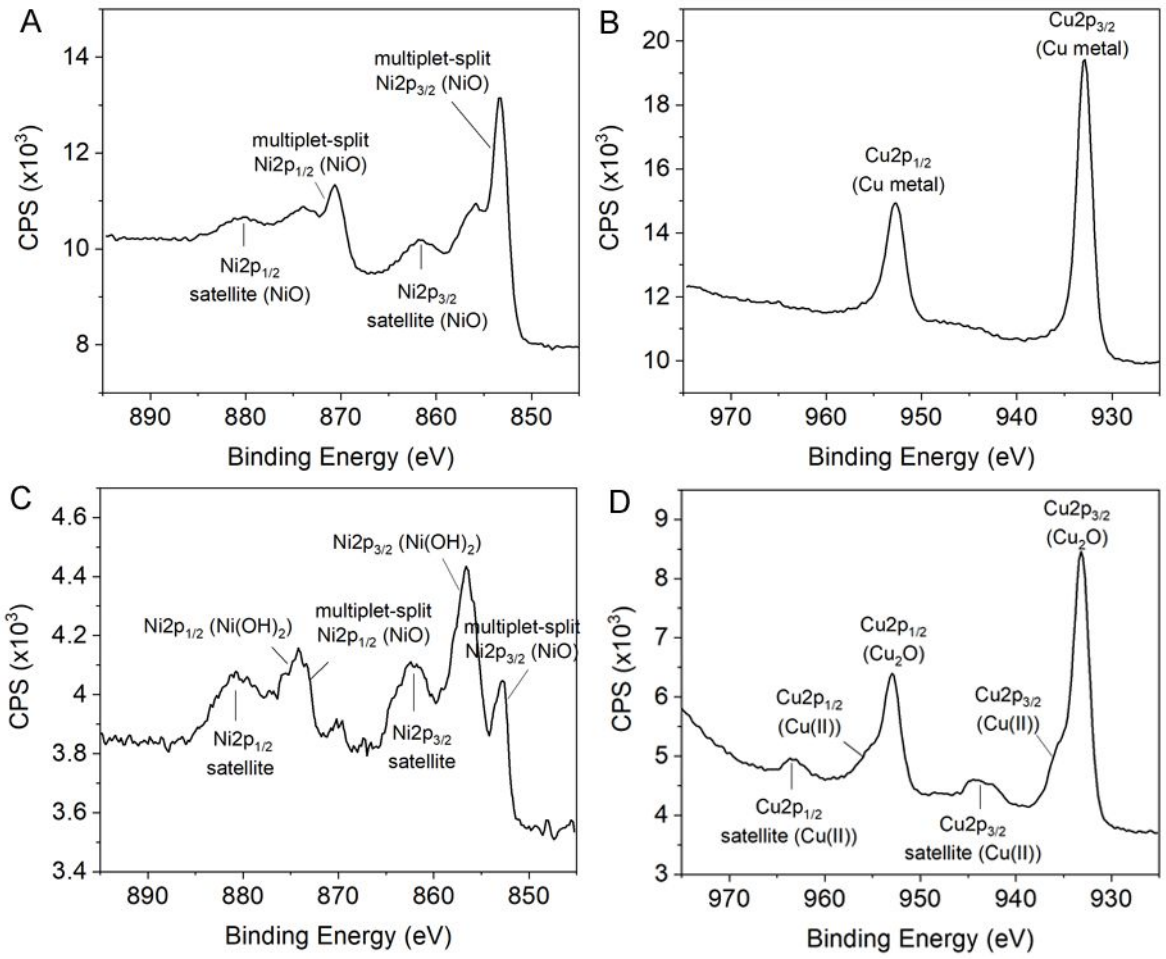

Figure S13. XPS spectra of the Cu-NiO_x core-shell structures and the CuNiOx hollow structures: Ni2p spectrum (A) and Cu2p spectrum (B) of the Cu-NiO_x core-shell structures; and Ni2p spectrum (C) and Cu2p spectrum (D) of the $CuNiO_x$ hollow structures. Note that the Cu2p of Cu metal and the Cu2p in Cu_2O overlap in XPS but the assignments can be made based on XRD results. The Cu2p for the Cu core in core-shell structures is assigned to Cu metal because of the existed fcc Cu metal in their XRD pattern (Figure S9B, black curve) while the Cu2p in the hollow structures is assigned to Cu_2O due to the lack of diffraction patterns in the XRD of the hollow structures (Figure S9B, blue curve). Compared to the core-shell structure, the surfaces of the hollow structures were converted from oxides to hydroxides because of the NH_4OH treatment in the etching process.

References:

1. Biesinger, M. C.; Payne, B. P.; Grosvenor, A. P.; Lau, L. W.; Gerson, A. R.; Smart, R. S. C., Resolving Surface Chemical States in Xps Analysis of First Row Transition Metals, Oxides and Hydroxides: Cr, Mn, Fe, Co and Ni. *Appl. Surf. Sci.* **2011**, *257*, 2717-2730.
2. Goh, S. W.; Buckley, A. N.; Lamb, R. N.; Rosenberg, R. A.; Moran, D., The Oxidation States of Copper and Iron in Mineral Sulfides, and the Oxides Formed on Initial Exposure of Chalcopyrite and Bornite to Air. *Geochim. Cosmochim. Acta* **2006**, *70*, 2210-2228.